Mechanism of solid-state amorphization of Se induced by mechanical milling

Cite as: Journal of Applied Physics **95**, 7674 (2004); https://doi.org/10.1063/1.1737478
Submitted: 12 January 2004 • Accepted: 12 March 2004 • Published Online: 04 June 2004

Y. H. Zhao, Y. T. Zhu and T. Liu

Mechanism of solid-state amorphization of Se induced by mechanical milling

Y. H. Zhao and Y. T. Zhu[a)]
Materials Science and Technology Division, Los Alamos National Laboratory, Los Alamos, New Mexico 87545

T. Liu
Synchrotron Radiation Laboratory, Institute of High Energy Physics, Chinese Academy of Sciences, Beijing 100039, People's Republic of China

(Received 12 January 2004; accepted 12 March 2004)

In this work, the solid-state amorphization process of elemental trigonal Se via mechanical milling was studied. Trigonal Se has a unique crystal structure consisting of helical $[-\mathrm{Se}-]_n$ chains with strong intrachain covalent bonds and with weak interchain van der Waals bonds. It was found that the interchain coordination distance increased while the intrachain coordination distance decreased with increasing milling time. The crystalline Se transformed to the amorphous state once the interchain coordination distance reached a critical value. The intrachain coordination distance of amorphous Se continued to decrease with milling time, suggesting that molecular chain length decreased with milling time. Combined with the x-ray absorption near-edge structure calculations, it was concluded that the mechanical milling destroyed the interchain bonds of crystalline Se, resulting in the amorphization, while the intrachain bonds were strengthened during amorphization. The present results support a previous crystallite-destabilization model for solid-state amorphization. © *2004 American Institute of Physics.* [DOI: 10.1063/1.1737478]

I. INTRODUCTION

Recently, ball-milling-induced solid-state amorphization (SSA, or crystalline-to-amorphous phase transformation) has received considerable scientific attention because the combination of ball milling and subsequent consolidation may offer a way to produce technologically useful bulk amorphous materials.[1] To date, the SSA process has been observed in many binary alloy systems by mechanical alloying (MA) of corresponding elemental crystalline powder mixtures[2–6] or by mechanical milling (MM) of intermetallic compounds.[7–11] In the former case, it has been observed that a negative heat of mixing and fast diffusion of one of the elements favor the formation of amorphous alloy phases, and that the kinetics of the amorphization process is controlled by the solid-state interdiffusion reaction.[5] In the latter case, the MM process induces accumulations of lattice defects and/or chemical disorders that raise the free energy of the milled system to above that of the amorphous state, leading to a collapse of the crystalline structure.[3]

Besides the amorphization of mixtures of elements by MA and intermetallic compounds by MM, the SSA process was also observed in some covalently bonded pure elements, such as Si,[12–14] Ge,[15] and Se.[16,17] Among these pure elements, trigonal Se (t-Se) is the only one that can be fully amorphized, due to its special molecular structure. As shown in the inset[19] in Fig. 1, t-Se consists of helical $[-\mathrm{Se}-]_n$ molecular chains. Se atoms in the molecular chain are bonded by strong covalent bond, and atoms between the adjacent $[-\mathrm{Se}-]_n$ molecular chains are bonded with weak van der Waals forces.[20] Within a $[-\mathrm{Se}-]_n$ chain, the first nearest-neighboring coordination distance is 2.374 Å (such as the A–B bond in Fig. 1), and the second intrachain coordination distance is 3.717 Å (A–C bond). Between the adjacent $[-\mathrm{Se}-]_n$ chains, the first nearest-neighboring coordination distance is 3.436 Å (such as the A–B* bond), and the second interchain coordination distance is 4.366 Å (A–A* bond). In previous work, quantitative x-ray diffraction (XRD) measurements on the MM-induced SSA of t-Se indicated that the amorphization onset corresponds to the critical values of crystallite size and lattice expansion as well as a maximum microstrain.[18] Infrared and Raman spectroscopy analyses revealed that the as-milled amorphous Se is mainly composed of the disordered $[-\mathrm{Se}-]_n$ polymeric chains.[21] These results imply that the MM process introduced lattice defects (such as grain boundaries, dislocations, vacancies, etc.) into t-Se, and when the accumulation of the lattice defects reached a critical value, the ordered $[-\mathrm{Se}-]_n$ molecular chains destabilized into the disordered $[-\mathrm{Se}-]_n$ polymeric chains. However, a systematic investigation on the local structural evolutions of intra- and inter- $[-\mathrm{Se}-]_n$ chains (e.g., the coordination distance and the disorder factor) during the MM-induced SSA process is still lacking.

In this work, low-temperature extended x-ray absorption fine-structure (EXAFS) analysis was employed to investigate the local structural evolutions of the intra- and inter- $[-\mathrm{Se}-]_n$ chain bonds during amorphization. In addition, the Se x-ray absorption near-edge structure (XANES) spectra was calculated to compare with the experimental absorption spectra. The mechanisms of MM-induced amorphization of Se were discussed based on these results.

a)Electronic mail: yzhu@lanl.gov

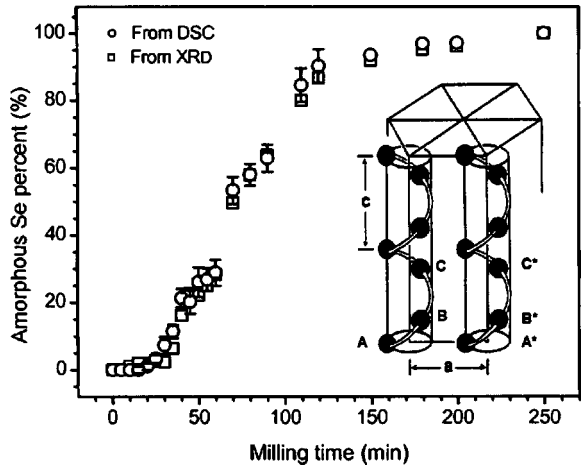

FIG. 1. Milling time dependence of the amorphous Se percent in the milled Se samples calculated from x-ray diffraction (XRD, empty squares) and differential scanning calorimeter (DSC, empty circles) analyses (Ref. 18) and the schematic representation of the helical trigonal Se structure (Ref. 19).

II. EXPERIMENTAL PROCEDURES

A. Sample preparation

Mechanical milling of pure Se powders (with a purity of 99.999% and particle size smaller than 600 mesh) was carried out in a high-energy vibratory ball mill with stainless-steel balls and vial at ambient temperature. The ball-to-powder weight ratio was 10 to 1. To avoid oxidation, about 4.5 g Se powder was charged into the vial and sealed by an elastic O-ring under dry Ar atmosphere (O_2, $H_2 < 5$ ppm) with an overpressure of about 3 atm. Each mechanical milling procedure was started with a new batch of initial powder and was carried out without interruption. Previous XRD and differential scanning calorimeter (DSC) analyses[18] indicated that the amorphization of *t*-Se starts at 30 min and finishes at 250 min (as shown in Fig. 1). Wet chemical analysis and energy-dispersive x-ray analysis indicated that the O content was less than 0.1 wt % and the Fe content less than 0.02 wt % in the sample milled for 250 min.

B. EXAFS measurements

EXAFS measurements were carried out on the 4W1B beam-line of the Beijing Synchrotron Radiation Facility for High-Energy Physics (using 40 bending magnets) when the facility was under dedicated running conditions. The storage ring current was 50–80 mA at 2.2 GeV. A directly water-cooled Si(111) double-crystal monochromator provides a stable and intense incident photon beam with energies ranging from 3.5 to 22 keV and an energy resolution of about 2 eV at 9 keV.

To measure the amplitude of the EXAFS precisely, considerable attention was given to avoid experimental problems that can cause amplitude distortion,[22] including the preparation of homogeneous sample and the minimization of the absorption of high-energy x-ray harmonics. Taking care of the severe thickness requirement (about 1 absorption length thick: approximate 27 μm for Se) and homogeneity requirement for the EXAFS samples, the milled Se powders were spread uniformly on a special translucent adhesive tape, and six layers of the tape were stacked together for accurate EXAFS measurements. The particle sizes of the as-milled and unmilled powders (less than 15 μm) were less than 1 absorption length thick, and therefore, the amplitude distortion caused by the thickness effect of the powders is negligible.[23] In order to minimize the absorption of high-energy x-ray harmonics, the monochromator was detuned about 30% so that the high-energy harmonics had negligible intensity, and the ion chamber filling gases were selected carefully. The ion chamber monitoring the incident x-ray beam was filled with Ar and the ion chamber monitoring the transmitted x-ray beam filled with a mixture of Ar (75 vol. %) and N_2 (25 vol. %). The Se *K*-edge absorption spectra were finally recorded at liquid nitrogen temperature (77 K, in order to increase the available *k* space) using transmission mode by the ion chamber detectors.

III. CALCULATION

The calculations of Se XANES spectra were carried out based on the one-electron full multiple-scattering (MS) theory.[24,25] The Mattheiss prescription[26] was used to construct the cluster electronic density and the Coulomb part of the potential by superposition of neutral atomic charge densities obtained either from the Clementi–Roetti tables[27] or generated by the atomic relativistic Hartree–Fock–Slater code of Desclaux.[28] In order to simulate the charge relaxation around the core hole in the photoabsorber of atomic number *Z*, the screened $Z+1$ approximation (final state rule) was used, which consists of taking the orbitals of the $Z+1$ atom and constructing the final state charge density by using the excited configuration of the photoabsorber with the core electron promoted to a valence orbital.[29] For the exchange-correlation part of the potential, the energy- and position-dependent complex Hedin–Lundquist (H–L) self-energy $\Sigma(\mathbf{r},E)$ were used, as described by Tyson *et al.*[30] The imaginary part of the H–L potential gives the amplitude attenuation of the excited photoelectronic wave due to extrinsic inelastic losses, and automatically takes into account the photoelectron mean-free path in the excited final state. The calculated spectra are further convoluted with a Lorentzian function with a full width $\Gamma_h(=3.3\,\mathrm{eV})$ to account for the core hole lifetime.[31]

IV. RESULTS

A. XANES results

Figures 2(a) and (b) show the MS theoretical computations of the Se *K*-edge XANES spectra for *t*-Se using different cluster sizes (3, 9, 55, and 97 atoms). Figure 2(b) is the Lorentzian convolution of Fig. 2(a). For a minimal cluster composed of a Se central atom (emitter) surrounded by the two intrachain first-nearest-neighboring Se atoms, the calculated absorption spectrum shows the presences of the peaks *A* and *C*. With increasing number of atoms up to nine in the cluster (one central Se plus two intrachain first coordination Se, four interchain first coordination Se, and two intrachain second-nearest-neighboring Se atoms), peak *B* appears, arising mainly from the interchain interactions. For the 55- and

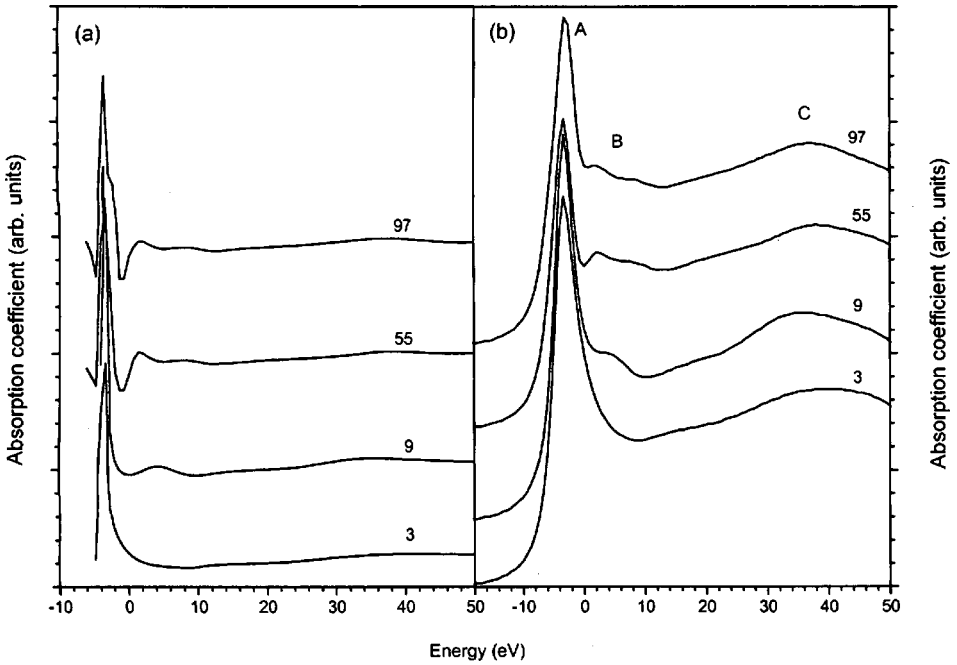

FIG. 2. Theoretical XANES spectra at the Se K edge of trigonal Se as a function of cluster size (clusters composed of 3, 9, 55, and 97 atoms, respectively). Figure (b) is the Lorentzian function convolution of Fig. (a).

97-atom large clusters, peak B was split into two peaks (corresponding to the interchain first coordination Se and intrachain second-nearest-neighboring Se atoms, respectively), and the intensity of peak C increases slightly, due to the multiple scattering of several $[-\mathrm{Se}-]_n$ molecular chains.

B. EXAFS results

1. EXAFS spectra

Figure 3(a) shows the measured Se K-edge x-ray absorption spectra for samples subjected to different milling periods. This figure shows an excellent signal-to-noise ratio. With increasing incident x-ray energy, the absorption coefficients of all measured Se samples increased sharply to a maximum at the Se K-absorption edge E_0, arising from the transfer of an electron from the $1s$ to $4p$ orbital, and then exhibit periodic oscillations when the x-ray energy is larger than E_0. Figure 3(b) represents the amplified K-edge absorption spectra of the milled Se near E_0. With increasing milling time t_m, peak B became sharper, and peak C became weaker; while peak A was nearly unchanged. Comparing the experimental Se K-edge x-ray absorption spectra with the calculated Se K-edge XANES spectra [Fig. 2(b)], one can conclude that the MM process weakened Se interchain interaction.

Since the oscillatory part of the x-ray absorption spectra contains the local atomic structural information, we isolated

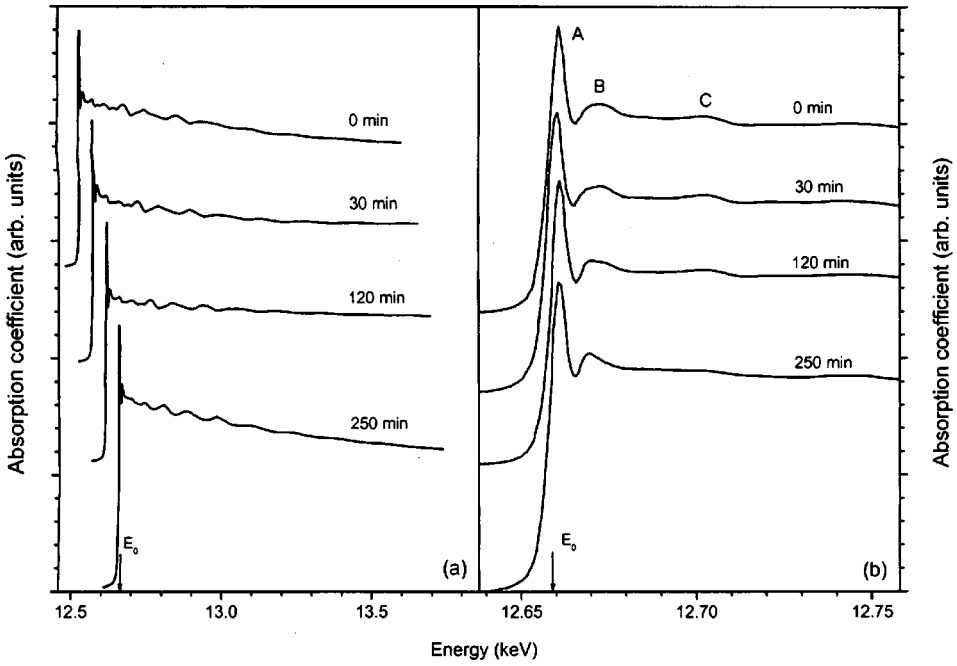

FIG. 3. (a) Se K-edge x-ray absorption spectra for the milled Se samples with different milling times (as indicated); the upper spectrum shifts about 50 eV towards the lower x-ray energy compared to the lower one. (b) The amplified K-edge absorption spectra of the milled Se near Se K-absorption edge E_0.

the x-ray absorption fine structure from the absorption spectra and inverted it to obtain the structural parameters. Details of the procedure are given in Refs. 32 and 33. Here, we only outline the procedure. First, the curve $a_1E^{-3}+a_2E^{-4}+a_3$, with photon energy E and parameters a_1, a_2, and a_3, was fitted to the smooth background caused by the atomic absorption in the pre-K-edge region. Another least-square spline was fitted with the background in the postedge region. The thickness parameter t was determined by equating the difference of the two polynomial curves to $t\cdot(C\cdot E^{-3}-D\cdot E^{-4})$, where C and D were given in Ref. 34, at a fixed point near K-edge. The EXAFS χ was derived by removing the least-square spline from the absorption spectra and subsequently by normalizing by $t\cdot(C\cdot E^{-3}-D\cdot E^{-4})$. The data after background removal and normalization were then converted to a function of the photoelectron wave number k, rather than as a function of energy. The conversion is $k=(2m(E-E_0)/\hbar^2)^{1/2}$, where E_0 was chosen at the top of the first peak in the absorption spectra in all samples and m the electron mass.

2. Fourier transformation

The converted EXAFS oscillations were multiplied by k^2, i.e., $k^2\chi(k)$ and were then converted from a representation in terms of k to that in coordinate space R by the Fourier transform[32,33] in the region extending from 2.6 to 16.0 Å^{-1}. The Fourier transform gives an immediate and graphic presentation of how many coordination shells are contributing to the EXAFS signal and their approximate distances. Typical results for the magnitude of the Fourier transformation $FT[k^2\chi(k)]$ for the milled Se samples are shown in Fig. 4. The prominent peak A observed at about 2.3 Å corresponds to the intrachain first-nearest coordination shell. Peak B is due to the interchain first-nearest-neighboring Se atoms (at about 3.4 Å) and the intrachain second-nearest-neighboring Se (at about 3.7 Å). Peak C at about 4.4 Å corresponds to the interchain second-nearest coordination shell. With increasing t_m, peaks B (or more strictly, the part of peak B corresponding to the interchain first coordination shell at 3.4 Å) and peak C became significantly weaker, and the sample milled for 250 min exhibits a typical amorphous feature of the short-range ordered structure. Peak A has no evident change during the milling process. These results indicate that the mechanical milling process destroyed the interchain interaction of t-Se and made the interchain neighbors spread over a wide range of separation distances. The interchain interactions would then be undetectable by EXAFS, decreasing the intensities of peaks B and C.

3. Coordination distances

In order to obtain the structural parameters of different coordination shells of the milled Se, whole-spectra fitting was performed on the Fourier transformed data, as shown by the solid lines in Fig. 4. During the fitting, the phase difference and the backscattering amplitude were calculated from theory, the number of coordination shells was limited to four,

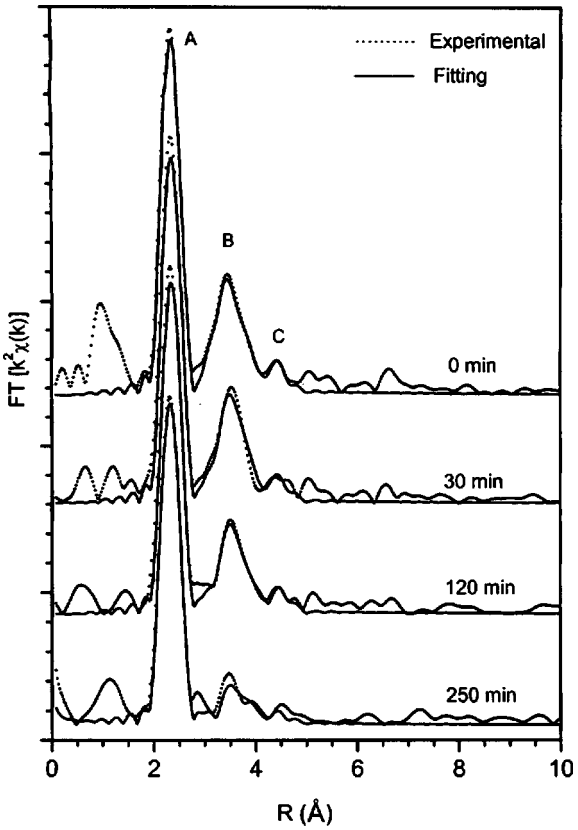

FIG. 4. Magnitude of Fourier transform of the Se K-EXAFS oscillations multiplied by k^2, $FT[k^2\chi(k)]$, for the milled Se. The transform range was from 2.6 to 16.0 Å^{-1}. The dot lines are the experimental results and the solid lines are the fitted results.

and the coordination number of each coordination shell was fixed. The fitting results were listed in Table I and plotted in Figs. 5(a)–(d) and Fig. 6.

From Figs. 5(a) and (c), during the whole milling process, the intrachain first- and second-nearest-neighboring coordination distances l_1 (such as the A–B bond) and l_3 (A–C bond) of the milled Se samples decrease gradually from 2.38 ±0.01 Å (0 min) to 2.35±0.01 Å (250 min) and from 3.73 ±0.02 Å (0 min) to 3.69 Å (250 min), respectively. The l_1 reduction amplitude is larger than experimental uncertainty, while the l_3 variation is within the error bar. In the literature, the l_1 of t-Se is reported to be 2.37±0.02 Å,[35] 2.36±0.01 Å,[36] and 2.370±0.002 Å,[37] which agree with the present value of the unmilled t-Se (2.38±0.01 Å). Neutron diffraction analysis found that the l_1 value of the as-milled amorphous Se, which was prepared by mechanical alloying of Se and S mixtures, is 2.346±0.002 Å.[37] This value is comparable to the present l_1 value of the as-milled amorphous Se (2.35±0.01 Å). Moreover, the l_1 of the as-milled amorphous Se is also comparable with the l_1 of the as-quenched amorphous Se, which is found to be 2.35±0.02 Å.[35]

The first intrachain distance l_1^t of t-Se has the following relation with the lattice parameters a and c:[20]

$$l_1^t=\sqrt{(c/a)^2+(ma)^2}. \tag{1}$$

Therefore, according to Eq. (1), with $l_1^0=2.374$ Å, $a_0=4.3662$ Å, $c_0=4.9536$ Å ($m=0.3903$), and using the mea-

TABLE I. The coordination distances l and disorder factors σ^2 for the first, second, third, and fourth coordination shells of the milled Se samples with coordination numbers N of 2, 4, 2, and 6, respectively. The error bars are estimated to be 0.01 Å and 10% for l and σ^2 of the first and second coordination shells, respectively. For the l and σ^2 of the third and fourth coordination shells, the error bars are estimated to be about 0.02 Å and 20% because of the weak EXAFS signal. For the sample milled 250 min, except for the first shell, the errors for the other shells are estimated larger than 0.02 Å and 20% for l and σ, respectively.

Milling time (min)	N	l (Å)	σ^2 (10^{-3},Å^2)
	2	2.38	2
0	4	3.37	13
	2	3.73	9
	6	4.37	23
	2	2.38	2
20	4	3.38	14
	2	3.72	9
	6	4.38	25
	2	2.37	3
30	4	3.39	15
	2	3.72	8
	6	4.38	26
	2	2.37	3
120	4	3.40	19
	2	3.70	10
	6	4.38	27
	2	2.35	3
250	4	3.41	35
	2	3.69	13
	6	4.38	38

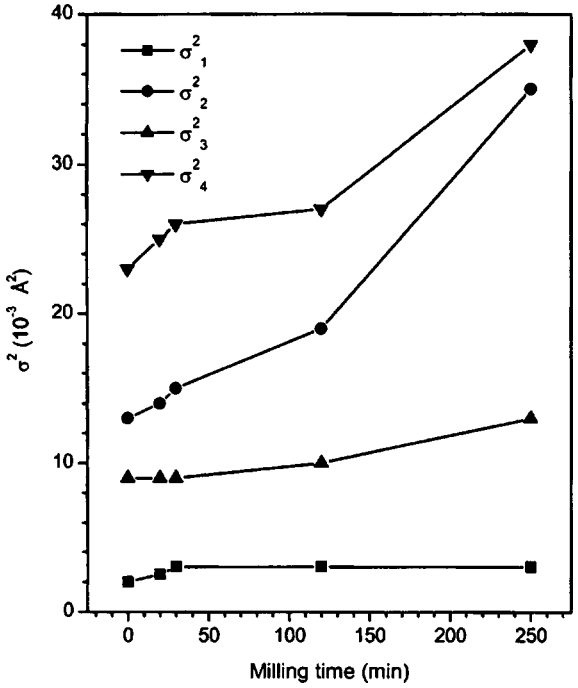

FIG. 6. The disorder factors of first, second, third, and fourth coordination shells σ_1^2, σ_2^2, σ_3^2, and σ_4^2 of the milled Se samples as a function of milling time.

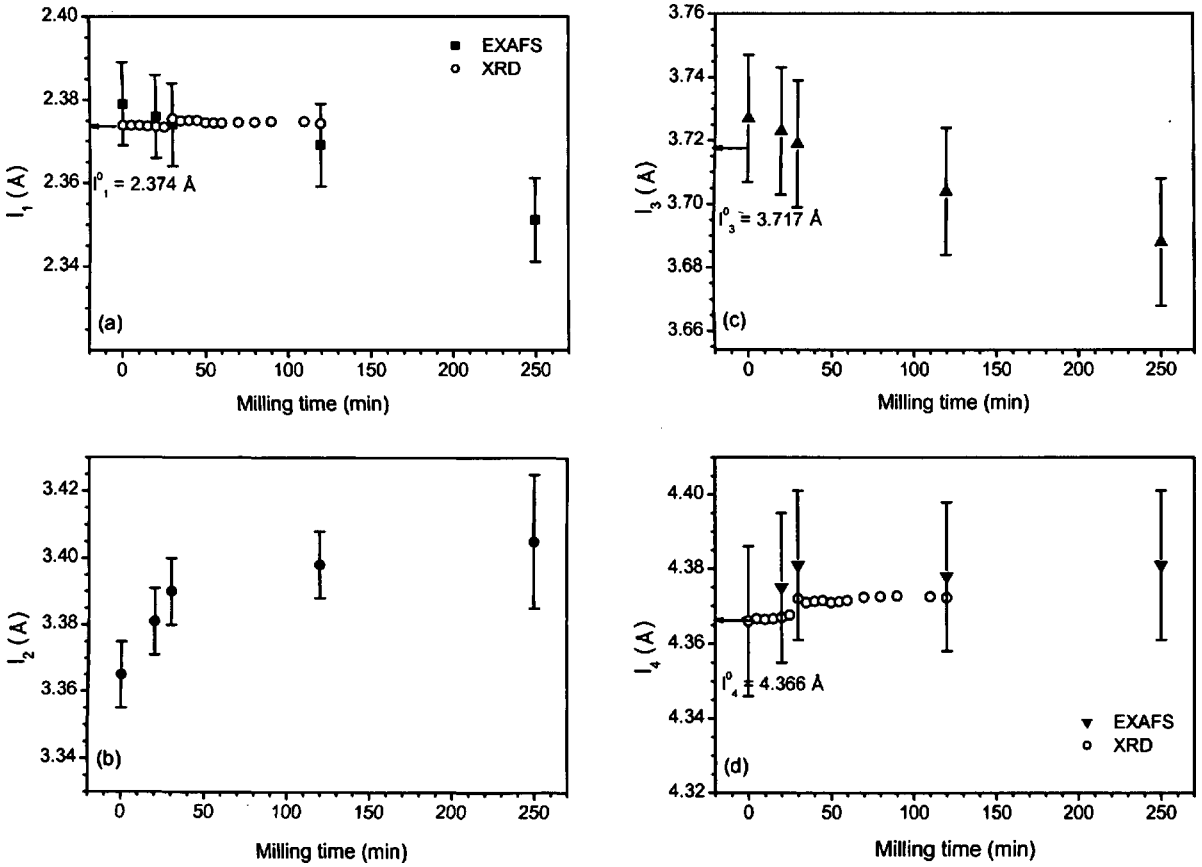

FIG. 5. Milling time dependences of the intrachain first (a) and second (c) coordination distances l_1 and l_3, and the interchain first (b) and second (d) coordination distances l_2 and l_4 for the milled Se samples obtained from EXAFS analysis (solid symbols). The empty circles are the coordination distances of t-Se in the milled powders obtained from XRD measurements (Ref. 18).

sured lattice parameters, the l_1^t of t-Se in the milled Se powders can be calculated. The lattice parameters a and c of the t-Se in the milled Se powders were calculated from XRD peak centroid positions[38] and were reported in Ref. 18. The calculated l_1^t of t-Se [using the lattice parameter values from Ref. 18 and Eq. (1)] in the milled Se powders is also shown in Fig. 5(a). The l_1^t remains unchanged during the main amorphization process and agrees with the standard value ($l_1^0 = 2.374$ Å) in the literature. The l_1 obtained from the EXAFS measurements (written as $l_1^{\text{mix.}}$) is the average of both t-Se and amorphous Se, because the ball-milling process did not destroy the intrachain bonds, and the intrachain interaction of amorphous Se can be detected by EXAFS. Therefore, the following simple rule-of-mixture equation can be used: $l_1^{\text{mix.}} = l_1^t(1-x) + l_1^a x$, where x is the fraction of amorphous Se, and l_1^a is the first intrachain distance of amorphous Se. When $t_m = 120$ min, l_1^a can be calculated to be 2.368 Å with the values of $x = 88.6\%$, $l_1^{\text{mix.}} = 2.369$ Å, and $l_1^t = 2.374$ Å. The measured value of l_1^a when $t_m = 250$ min (2.351 Å) is much smaller than the value of l_1^a calculated from the rule of mixture when $t_m = 120$ min. This suggests that with increasing ball-milling time, the intrachain coordination distance of amorphous Se was shortened.

From Figs. 5(b) and (d), during grain-refinement process (0–30 min), the interchain first- and second- coordination distances l_2 (A–B* bond) and l_4 (A–A* bond) increased from 3.37±0.01 Å (0 min) to 3.39±0.01 Å (30 min) and from 4.37±0.02 Å (0 min) to 4.38±0.02 Å (30 min), respectively. The variation of l_2 is within the experimental error bar, and the l_4 variation is beyond the experimental uncertainty. However, during the amorphization process (30–250 min), l_2 and l_4 remain nearly unchanged. The l_4 value of the unmilled t-Se is comparable with the literature value l_4^0 (=4.366 Å), while l_2 of the unmilled t-Se is less than l_2^0 (=3.436 Å). The measured l_4 of t-Se in the milled powders from XRD[18] were also shown in Fig. 5(d). The l_4 obtained from XRD has similar variations to the EXAFS-calculated l_4 against the milling time: increases to the maximum value at $t_m = 30$ min, and remains unchanged during the main amorphization process. The l_2 and l_4 obtained from the EXAFS measurements mainly correspond to the values of crystalline Se in the milled powders, because the interchain bonds of the as-milled amorphous Se were destroyed and undetectable. Therefore, the results from EXAFS and XRD agree with each other.

4. Disorder factors

As shown in Fig. 6, during the milling process the disorder factors of the intrachain first and second coordination shells σ_1^2 and σ_3^2 increase slightly from 0.002 Å^2 (0 min) to 0.003 Å^2 (250 min) and from 0.009 Å^2 (0 min) to 0.013 Å^2 (250 min), respectively. However, the disorder factors of the interchain first- and second coordination shells σ_2^2 and σ_4^2 increase significantly from 0.013 Å^2 to 0.035 Å^2 and from 0.023 Å^2 to 0.038 Å^2 with an increase in the milling time from 0 to 250 min. The increased amplitude of disorder factors of interchain coordination shells is much larger that of the intrachain coordination shells. The value of σ_1^2 is comparable with those in the literature, which are in a range from 0.001 Å^2 to 0.002 Å^2.[36]

V. DISCUSSION

It has been reported that as the MM-induced SSA of Se proceeded, the peak corresponding to the interchain first coordination (at approximate 3.4 Å) moved continuously to the peak position of the intrachain second coordination (at 3.7 Å).[16] However, in this study we did not observe this effect (see peak *B* in Fig. 4). We only observed that the intensity of peak *B* (the part corresponding to the interchain first coordination shell at about 3.4 Å) was decreased significantly during the amorphization process. This difference may be caused by different experimental conditions. In Ref. 16, a low-energy planetary ball-milling apparatus was used to realize the SSA of Se and the milling time for complete SSA is 50 h. In present work, a high-energy vibratory mill was employed and the complete SSA milling time is only about 4 h. Therefore, in the present work, the high-energy ball milling directly destroyed the interchain bonds (amorphization) and made them undetectable. Moreover, Guo *et al.* reported that the as-milled amorphous Se produced by low-energy planetary mill had the interchain interaction,[21] while the present as-milled amorphous Se by high-energy milling only had very weak interchain interaction, as verified by the Fourier transform of the sample milled for 250 min (Fig. 4).

A. Inter- $[-\text{Se}-]_n$ chain interaction

The present results demonstrate that the local structural parameters of both intra- and inter- $[-\text{Se}-]_n$ chains were changed during the MM-induced amorphization. The inter-$[-\text{Se}-]_n$ chain interaction was weakened by the milling process during the grain refinement ($t_m < 30$ min), resulting in the observed increases of the interchain coordination distances l_2 and l_4 [Figs. 5(b) and (d)]. The increase in l_2 and l_4 mainly originated from the strong interaction between the numerous grain boundaries and nanometer-sized crystallites, which was verified in Ref. 38. When $t_m = 30$ min, the grains were refined to the minimal value,[18] and the interchain coordination distances l_2 and l_4 were increased to the critical values where the ordered $[-\text{Se}-]_n$ chains can be destabilized to become disordered chains (crystallite destabilization model, which was described in detail in Ref. 18). During the SSA process ($t_m > 30$ min), the $[-\text{Se}-]_n$ chains destabilized into the disordered chains, resulting in the observed evident increase in interchain disorder factors σ_2^2 and σ_4^2 (Fig. 6) as well as the significant decreases in the interchain coordination peaks *B* and *C* (Fig. 4). The preferential destruction of interchain bonds can be qualitatively understood by the fact that the interchain van der Waals force is much weaker than the intrachain covalent bond.

B. Intra- $[-\text{Se}-]_n$ chain interaction

The intra- $[-\text{Se}-]_n$ chains bonds were also changed during the mechanical milling (SSA) process. The observed shorter intrachain coordination distances l_1 and l_3 [Figs. 5(a) and (c)] indicate that the intrachain covalent bond was

strengthened. The bond length shortening can be understood by the weakened and/or destroyed interchain bonds due to MM. The helical molecular chain structure in *t*-Se originates from minimization of the intra- and interchain repulsive interactions. The MM process weakens and/or destroys the interchain bonds; therefore, the intrachain interaction was strengthened in order to reach a new stable state. On the other hand, the structural disorder in the amorphous Se relaxed the folded spiral chain. As a result of decreased Coulomb repulsion, this would increase the overlap integral, or the bond charge, and consequently shorten the bond length. In addition, the shortening of the chain length induced by the milling process can also result in the shortening of intrachain bond length. In has been reported that the ball milling broke the $[-\mathrm{Se}-]_n$ chain, reducing the atom number in one chain.[37] The slight increases of the intrachain disorder factors may result from the structural defects induced by the milling process.

VI. CONCLUSIONS

In summary, low-temperature EXAFS measurements on MM-induced SSA of *t*-Se and Se *K*-edge XANES spectra calculations indicated that the amorphization onset corresponds to critical interchain coordination distances. The SSA process was accompanied by reduction of the intrachain coordination distances and the interchain coordination peak intensities, as well as the increases of the interchain disorder factors. These results lead to the conclusion that the mechanical milling destroyed the interchain interaction of *t*-Se, resulting in the amorphization, while strengthening the intrachain interaction. The present observations support our previous crystallite-destabilization model for amorphization.

[1] C. Suryanarayana, Prog. Mater. Sci. **46**, 1 (2001).
[2] W. L. Johnson, Prog. Mater. Sci. **30**, 81 (1986).
[3] R. B. Schwarz and C. C. Koch, Appl. Phys. Lett. **49**, 146 (1986).
[4] E. Hellstern and L. Schultz, Mater. Sci. Eng. **97**, 39 (1988).
[5] L. Schultz, J. Less-Common Met. **145**, 233 (1988).
[6] A. W. Weeber and H. Bakker, Physica B **153**, 93 (1988).
[7] A. Ye. Yermakov, Ye. Ye. Yurchikov, and V. A. Barinov, Phys. Met. Metallogr. **52**, 50 (1981).
[8] C. Polistis and W. L. Johnson, J. Appl. Phys. **60**, 1147 (1986).
[9] E. Gaffet, N. Merk, G. Martin, and J. Bigot, J. Less-Common Met. **145**, 251 (1988).
[10] J. S. C. Jang and C. C. Koch, J. Mater. Res. **5**, 498 (1990).
[11] Y. S. Cho and C. C. Koch, J. Alloys Compd. **194**, 287 (1993).
[12] E. Gaffet and M. Harmelin, J. Less-Common Met. **157**, 201 (1990).
[13] T. D. Shen, C. C. Koch, T. L. McCormick, R. J. Memanich, J. Y. Huang, and J. G. Huang, J. Mater. Res. **10**, 139 (1995).
[14] J. Y. Huang, H. Yasuda, and H. Mori, Philos. Mag. Lett. **79**, 305 (1999).
[15] E. Gaffet, Mater. Sci. Eng., A **136**, 161 (1991).
[16] T. Fukunaga, M. Utsumi, H. Akatsuka, M. Misawa, and U. Mizutani, J. Non-Cryst. Solids **205–207**, 531 (1996).
[17] G. J. Fan, F. G. Guo, Z. Q. Hu, M. X. Quan, and K. Lu, Phys. Rev. B **55**, 11010 (1997).
[18] Y. H. Zhao, Z. H. Jin, and K. Lu, Philos. Mag. Lett. **79**, 747 (1999).
[19] H. M. Isomäki and J. von Boehm, Phys. Rev. B **35**, 8019 (1987).
[20] P. Ungar and P. Cherin, in *The Physics of Selenium and Tellurium*, edited by C. W. Cooper (Pergamon, Oxford, England, 1969), p. 223.
[21] F. Q. Guo and K. Lu, Phys. Rev. B **57**, 10414 (1998).
[22] E. A. Stern and K. Kim, Phys. Rev. B **23**, 3781 (1981).
[23] K. Q. Lu and E. A. Stern, Nucl. Instrum. Methods **12**, 475 (1983).
[24] P. A. Lee and J. B. Pendry, Phys. Rev. B **11**, 2795 (1975).
[25] C. R. Natoli, D. K. Misemer, S. Doniach, and F. W. Kutzler, Phys. Rev. A **22**, 1104 (1980); C. R. Natoli, M. Benfatto, and S. Doniach, *ibid.* **34**, 4682 (1986).
[26] L. Mattheiss, Phys. Rev. A **134**, 970 (1964).
[27] E. Clementi and C. Roetti, At. Data Nucl. Data Tables **14**, 177 (1974).
[28] J. Desclaux, Comput. Phys. Commun. **9**, 31 (1975); J. Desclaux, J. Phys. B **4**, 631 (1971).
[29] P. A. Lee and G. Beni, Phys. Rev. B **15**, 2862 (1977).
[30] T. A. Tyson, K. O. Hodgson, C. R. Natoli, and M. Benfatto, Phys. Rev. B **46**, 5997 (1992), and references therein.
[31] J. C. Fuggle and J. E. Inglesfield, *Unoccupied Electronic States*, Topics in Applied Physics (Springer, Berlin, 1992), Appendix B, p. 347.
[32] E. A. Stern, D. E. Sayers, and F. W. Lytle, Phys. Rev. B **11**, 4836 (1975).
[33] E. A. Stern and S. M. Heald, in *Handbook of Synchrotron Radiation*, edited by E. E. Koch (North-Holland, Amsterdam, 1983), vol. 1B, Chap. 10.
[34] C. H. Macgillavry, C. D. Riech, and K. Lonsdale, *Int. Tables for X-ray Crystallography* (Kynoch, England, 1972), Vol. 3.
[35] Y. H. Zhao, K. Lu, and T. Liu, Phys. Rev. B **59**, 11117 (1999).
[36] A. V. Kolobov, H. Oyanagi, and K. Tanaka, Phys. Rev. B **55**, 726 (1997).
[37] T. Fukunaga, S. Kajikawa, Y. Hokari, and U. Mizutani, J. Non-Cryst. Solids **232–234**, 465 (1998).
[38] Y. H. Zhao, K. Zhang, and K. Lu, Phys. Rev. B **56**, 14322 (1997).